Journal of *Marine Science and Engineering*

MDPI

Article

Effect of Surfactants with Different Hydrophilic–Lipophilic Balance on the Cohesive Force between Cyclopentane Hydrate Particles

Qingchao Fang [1], Xin Zhao [1,2,*], Sunbo Li [1], Zhengsong Qiu [1,2], Zhiyuan Wang [1] and Qi Geng [1]

[1] School of Petroleum Engineering, China University of Petroleum (East China), Qingdao 266580, China
[2] Shandong Key Laboratory of Oilfield Chemistry, China University of Petroleum (East China), Qingdao 266580, China
* Correspondence: zhaoxin@upc.edu.cn

Abstract: Effective control of the cohesive force between hydrate particles is the key to prevent their aggregation, which then causes pipeline blockage. The hydrophilic–lipophilic balance (HLB) value of surfactants was proposed as an important parameter for the evaluation and design of hydrate anti-agglomerants. A microscopic manipulation method was used to measure the cohesive forces between cyclopentane hydrate particles in the presence of Tween and Span series surfactants with different HLB values; moreover, the measured cohesive force was compared with the results of calculations based on the liquid bridge force model. Combined with the surface morphology and wettability of the hydrate particles, we analyzed the mechanism by which surfactants with different HLB values influence the cohesion between hydrate particles. The results show that for both Tween (hydrophilic, HLB > 10) and Span (hydrophobic, HLB < 10) surfactants, the cohesive force between cyclopentane hydrate particles decreased with decreasing HLB. The experimental results were in good agreement with the results of calculations based on the liquid bridge force model. The cohesive force between hydrate particles increased with increasing concentration of Tween surfactants, while in the case of the Span series, the cohesive force decreased with increasing surfactant concentration. In the formation process of cyclopentane hydrate particles, the aggregation of low-HLB surfactant molecules at the oil–water or gas–water interface increases the surface roughness and hydrophobicity of the hydrate particles and inhibits the formation of liquid bridges between particles, thus reducing the cohesion between particles. Therefore, the hydrate aggregation and the associated blockage risks can be reduced.

Keywords: hydrate blockage; surfactants; HLB value; liquid bridge; cohesion force; surface wettability

Citation: Fang, Q.; Zhao, X.; Li, S.; Qiu, Z.; Wang, Z.; Geng, Q. Effect of Surfactants with Different Hydrophilic–Lipophilic Balance on the Cohesive Force between Cyclopentane Hydrate Particles. *J. Mar. Sci. Eng.* **2022**, *10*, 1255. https://doi.org/10.3390/jmse10091255

Academic Editor: Timothy S. Collett

Received: 27 July 2022
Accepted: 2 September 2022
Published: 6 September 2022

1. Introduction

Natural gas hydrates are crystalline clathrates formed by methane and other small-molecule hydrocarbon gases and water at high pressure and low temperature [1,2]. In the processes of drilling and exploitation of deep-sea oil, gas, and natural gas hydrates as well as oil/gas extraction and transportation, natural gas and water in the pipelines may generate or regenerate hydrates under low temperature and high pressure conditions. The hydrate particles continue to grow and accumulate, causing blockages and even safety issues [3,4]. At present, high concentrations of methanol, ethylene glycol, and sodium chloride hydrate are used as thermodynamic inhibitors to prevent hydrate plugging [5]. This approach presents many problems [6,7], such as large dosages of inhibitors, high costs, environmental pollution, and heavy logistic burden; hence, an environmentally friendly, low-dosage, and low-cost inhibitor is urgently needed to prevent wellbore plugging. Previous results show that the aggregation of hydrate particles as well as their cohesion and deposition on the pipe walls are the main causes of pipeline plugging [8–10]. Yuliev reported the use of surfactants to prevent hydrate aggregation. Subsequently, studies performed by the French Petroleum

Institute showed that non-ionic surfactants, including hydroxycarboxylic acid amides and polyalkoxy dihydroxyamides [11], could inhibit hydrate aggregation [12]. Shell Company researchers reported that quaternary ammonium salts with two or more *n*-butyl, *n*-pentyl, or isopentyl groups had a better anti-agglomeration effect; they developed anti-agglomerants based on single- and double-chain quaternary ammonium salts that were suitable for high supercooling conditions [13]; however, the biotoxicity and biodegradability of these agents could not meet the requirements of marine environmental protection [12]. It was found that rhamnolipid biosurfactants and sorbitan fatty acid ester surfactants could inhibit the aggregation of gas hydrates. The anti-agglomerants mentioned above can be used in oil–gas–water systems, but not in oil-free gas–water systems. Sun et al. [14] found that an anti-agglomerant containing cocamidopropyl dimethylamine as the main component could prevent hydrate aggregation in an oil-free gas–water system; Saikia et al. [15] reported that soybean lecithin can increase the aggregation time of tetrabutylammonium bromide (TBAB) hydrate crystals; Zhao et al. [16] found that an amphiphilic amide compound could inhibit the aggregation of hydrate particles in an oil-free gas–water system at 13 MPa and 2 °C.

No definitive consensus has yet been reached on the mechanism of action of hydrate anti-agglomerants. Kelland et al. [17,18] reported that surfactants can form water-in-oil emulsions in oil–water systems, preventing the contact of hydrate particles with water droplets. The patent of Shell Oil Company [13] reported that the hydrophilic groups of surfactants can adsorb on the surface of hydrate crystals, enhance the hydrophobicity of the hydrate surface, and facilitate the dispersion of hydrate particles in the oil phase. Huo et al. [19] tested several surfactants in high-pressure apparatuses, and the results indicated that the hydrophilic groups of surfactant molecules at the interface adsorb on the surface of hydrate particles and extend in the oil phase, resulting in steric hindrance between the particles and hindering their aggregation. Koh et al. [20] proposed that the hydrophilic groups of the anti-agglomerant could be intercalated into the hydrate crystal, resulting in defects that prevent the formation of larger particles. After measuring the adhesion forces between tetrahydrofuran hydrate particles, Taylor et al. [8] hypothesized that the surfactant molecules reduce the oil–water interfacial tension and weaken the capillary bridge force between hydrate particles, thus preventing particle aggregation. To sum up, anti-agglomerants mainly inhibit aggregation by reducing the oil–water interfacial tension [8], emulsifying droplets in oil–gas–water systems [17,18], altering the surface wettability of hydrate particles [19], and affecting their formation [20].

In order to further study the microscopic characteristics of anti-agglomerants preventing hydrate particles from aggregation, some researchers developed measurement systems to evaluate the cohesion between cyclopentane hydrate particles and analyze the mechanism of hydrate aggregation [21]. The microscopic manipulation experiments performed by Yang et al. [22] indicated that the cohesion between tetrahydrofuran (THF) hydrate particles decreases with decreasing temperature. Taylor et al. [8] improved the microscopic manipulation technique and found that the cohesion force between THF hydrate particles increases with increasing contact force and contact time. Experiments on CH_4/C_2H_6 hydrates also demonstrated that the interparticle force between particles increases with the contact time [23]; moreover, the interparticle force in liquid cyclopentane is independent of the effective radius of the particles, but in the gas phase, the same force is linearly related to the particle radius [24]. In addition, some chemicals, such as asphaltene, can prevent cyclopentane hydrate aggregation in oil–water systems [25].

The above analysis shows that some amphiphilic materials can inhibit the aggregation of hydrates. However, current studies of hydrate anti-agglomerants focus on the functional groups of amphiphilic materials that can be adsorbed on the surface of hydrates and aim to select amphiphilic anti-agglomerants that can prevent hydrate aggregation; no parameters or evaluation indicators that can directly guide the design and optimization of hydrate anti-agglomerants have been reported. Based on the surfactant theory and the analysis of the amphiphilic characteristics of hydrate anti-agglomerants, we selected Tween and Span surfactants to study the influence of different hydrophilic–lipophilic balance (HLB)

values on the cohesion between hydrate particles. The results show that the HLB value of surfactants can be used as an important parameter for the evaluation and design of hydrate anti-agglomerants. It provides theoretical guidance for the design and optimization of anti-agglomerants.

2. Materials and Methods

2.1. Materials

Span 80, Span 40, Span 20, Tween 60, and Tween 65 (purity $\geq$ 99.5%), as well as Tween 20 and Tween 65 (purity $\geq$ 99%) and cyclopentane (purity $\geq$ 99.5%) were purchased from Shanghai Macklin Biochemical Co., Ltd. (Shanghai, China); methane (purity $\geq$ 99.99%) was purchased from Qingdao Xinyuan Gas Co., Ltd. (Qingdao, China); deionized water was prepared in our laboratory.

2.2. Methods

Figure 1 shows the setup of the instruments used for measuring the cohesive force between hydrate particles. Among them, the microscope model we use is Leica S-APO, and the magnification can reach 80–220 times.

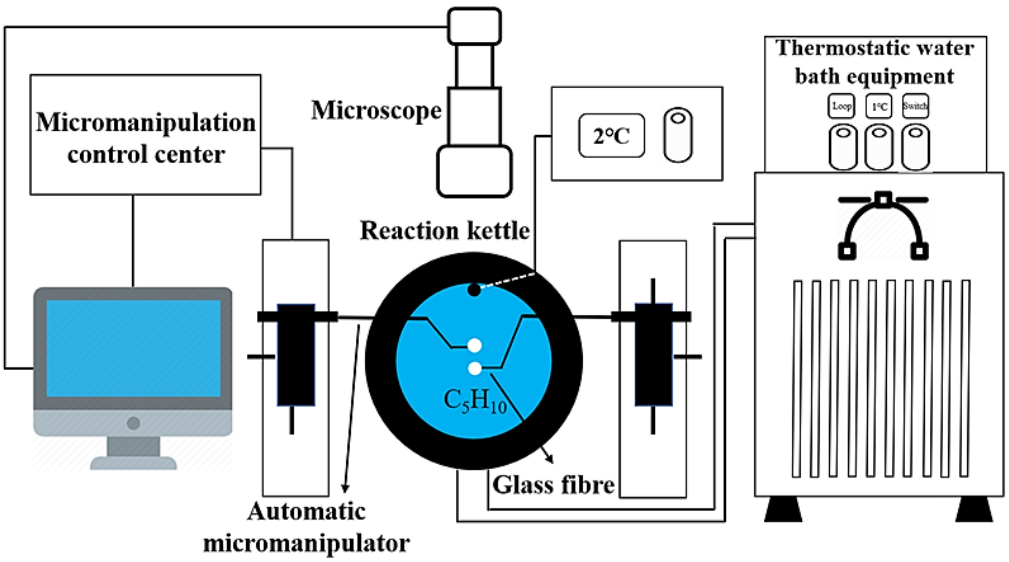

Figure 1. Apparatus used for measuring the cohesive force between hydrate particles.

Cyclopentane can form type II hydrates at atmospheric pressure and below 7.7 °C, which are of the same type as natural gas hydrates formed in wellbores, and can be tested at atmospheric pressure. The following experimental procedure was adopted. First, we took the two operating arms off the operating platform, fixed a drop of deionized water on the glass fiber at its end, and then placed it in liquid nitrogen for the 30 s to form ice particles. After that, we quickly installed the two operating arms on the operating platform; that is, we put the ice particles at the end of the glass fiber in the reaction kettle containing liquid cyclopentane and let it stand for 30 min at −1 °C, until it was converted into cyclopentane hydrate particles. Then, the cyclopentane hydrate particles in the reaction kettle were observed with a micro camera, and the cohesive force between them was measured by a pull-out method [26], as shown in Figure 2.

The hydrate particles fixed on a movable operation arm were set in contact with those on a fixed operation arm; then, a force of 2.2 mN·m was applied to the two hydrate particles for a contact time of 10 s; the half-filling angle α and the contact angle β of the liquid bridge between the particles were then measured, after which the movable arm was separated from the fixed arm at a speed of 1 μm/s. Due to the presence of the adhesive force between the particles, the glass fiber at the end of the fixed operating arm will bend, and the particles fixed on it will move together under the action of the cohesive force; the displacement of

the particles can then be measured. When the particle movement reaches a critical value (S) and continues to increase, the elastic force of the glass fiber is greater than the cohesion force; hence, the cohesion between the particles will be broken, and the two particles will be quickly separated under the action of the elastic force of the glass fiber.

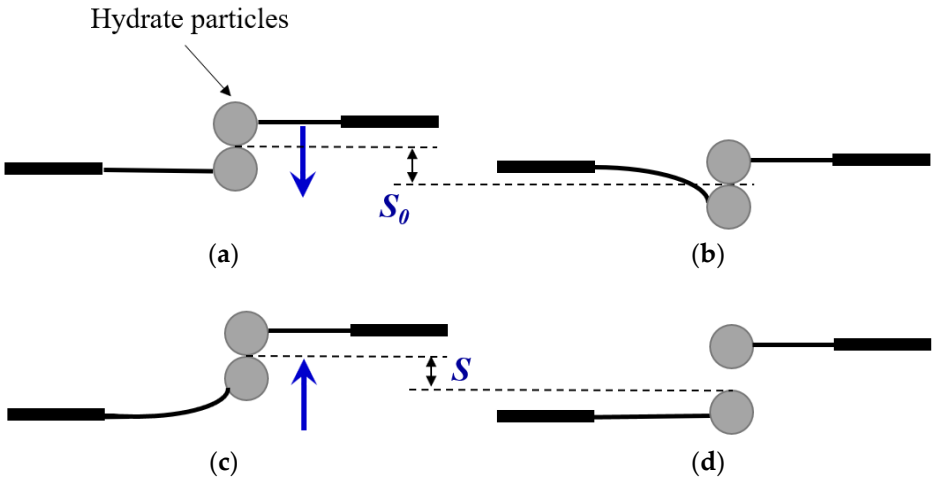

Figure 2. Schematic diagram illustrating the measurement of the cohesion between hydrate particles [16]: (**a**) hydrate particles approach; (**b**) contact and apply a force of 2.2 mN/m; (**c**) hydrate particles begin to separate; (**d**) critical position separation.

The cohesive force between the particles can be calculated according to Hooke's law:

$$F = kS \tag{1}$$

where F denotes the cohesive force (N), k denotes the elastic coefficient of the glass fiber, and S denotes the displacement (m).

In order to ensure the accuracy of the results, at least 40 repeated tests were carried out in each experiment. Because the diameters of hydrate particles prepared in each experiment were different, the harmonic mean radius R^* was used to normalize the results of the measurements. R^* was calculated as follows:

$$\frac{1}{R^*} = \frac{1}{2}\left(\frac{1}{R_1} + \frac{1}{R_2}\right) \tag{2}$$

where R_1 and R_2 are the radii of the two particles (m).

3. Results and Discussion

3.1. Cohesive Force between Cyclopentane Hydrate Particles

3.1.1. Measurement of Cohesive Force between Particles in the Presence of Surfactants with Different HLB Values

In order to explore the inhibition mechanism of hydrate aggregation by surfactants with different HLB values and rule out the influence of different functional groups on hydrate aggregation, Span (HLB < 10, hydrophobic) and Tween (HLB > 10, hydrophilic) surfactants with similar structural characteristics were selected to carry out micro-cohesion tests. By analyzing the influence of Span and Tween materials with different HLB values on the microscopic cohesive force between the hydrates, effective hydrate aggregation inhibitors could be designed and screened, as shown in Figures 3 and 4.

Figure 3 shows that compared with the pure cyclopentane hydrate particles, the interparticle cohesive force was reduced under the action of the Span 80, Span 40, and Span 20 surfactants with HLB values of 4.3, 6.7, and 8.6, respectively; moreover, the interparticle cohesive force decreased with increasing surfactant concentration, and the reduction extent was between 6% and 35% when the concentration was less than 0.5 wt.%. Span 80, with the lowest HLB value, had the strongest effect. The above results show that Span surfactants

could reduce the cohesion between the cyclopentane hydrate particles; moreover, at the same concentration, a lower HLB value resulted in a stronger effect.

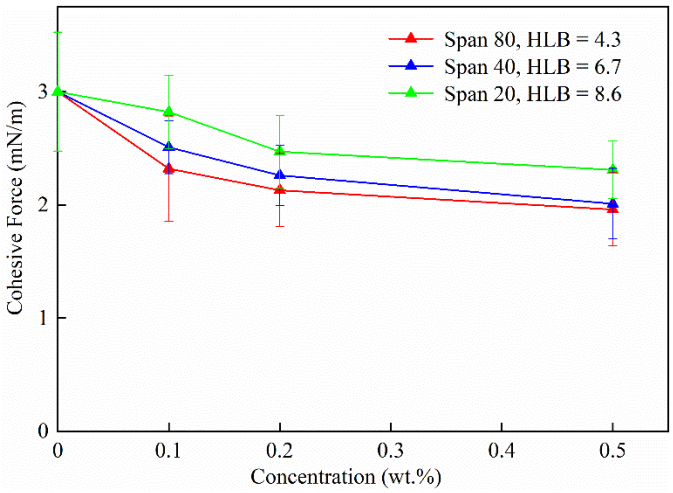

(**a**)

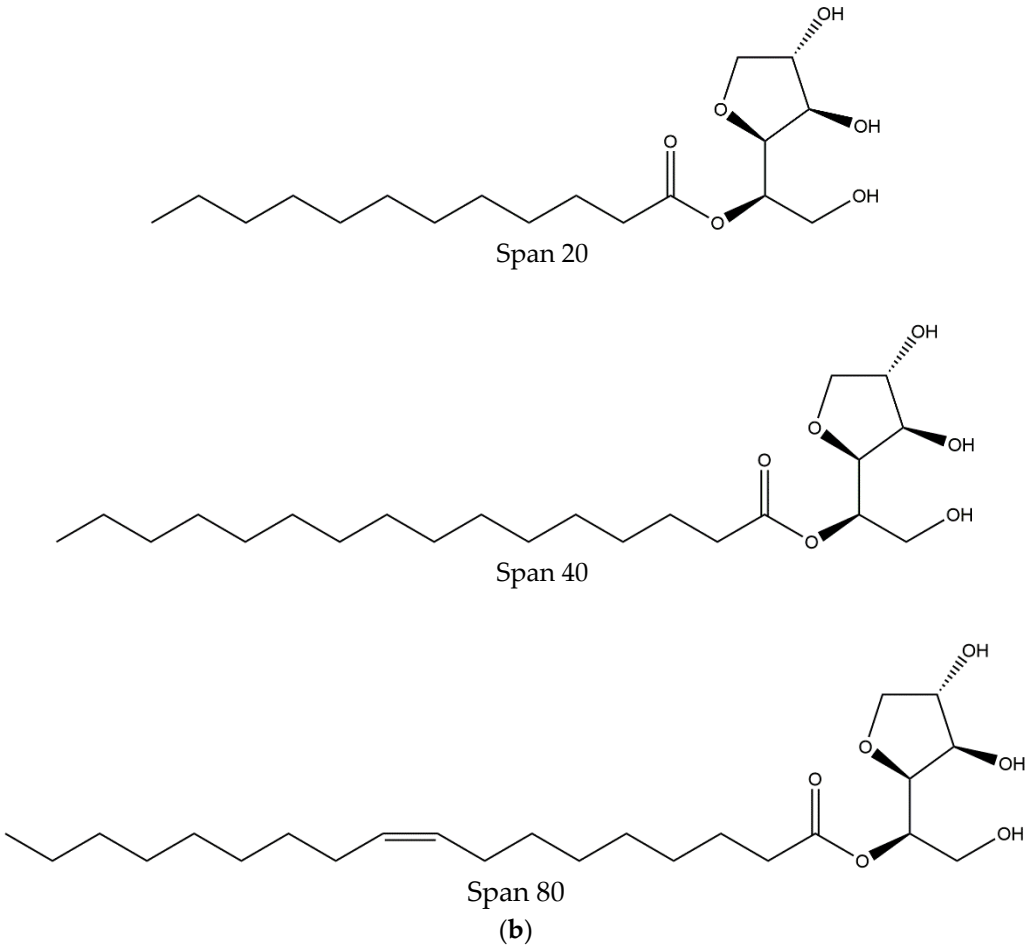

(**b**)

Figure 3. (**a**) Variation of cohesive force between hydrate particles with the concentration of Span surfactants (−1 °C, 2.2 mN/m, 10 s); (**b**) molecular structure diagram of Span series surfactants.

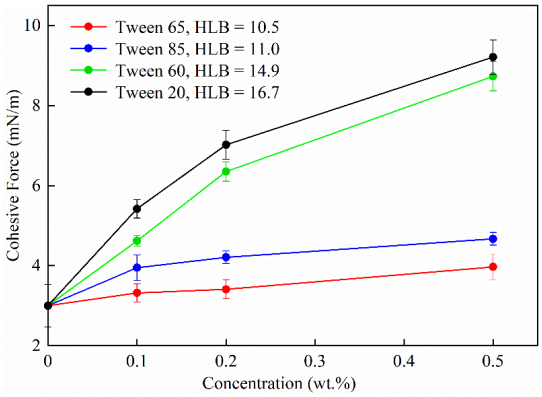

(**a**)

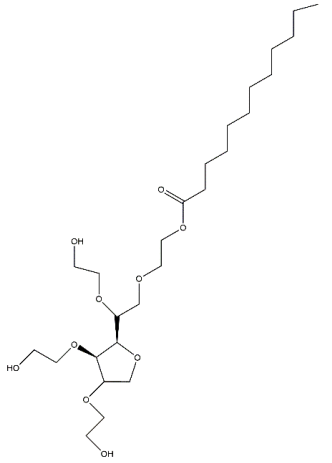

Tween 20

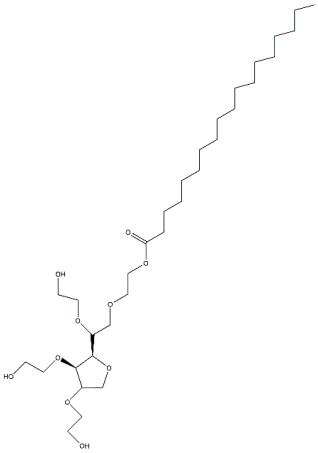

Tween 60

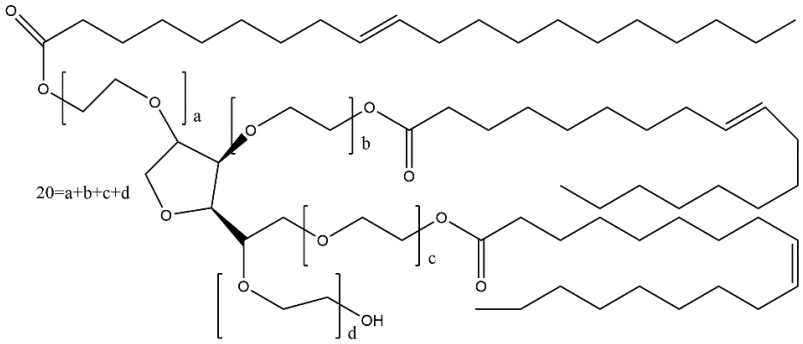

Tween 85

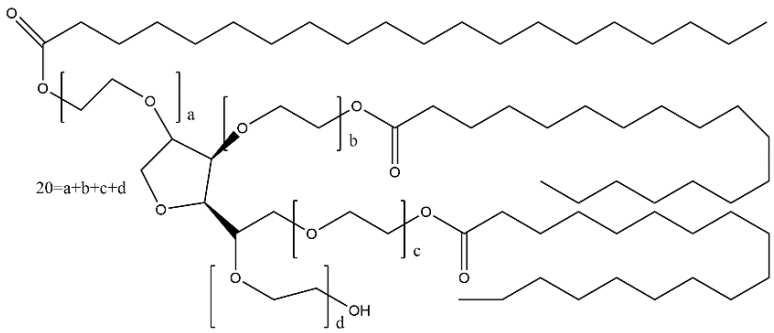

Tween 65

(**b**)

Figure 4. (**a**) Variation of cohesive force between hydrate particles with the concentration of Tween surfactants (−1 °C, 2.2 mN/m, 10 s); (**b**) molecular structure diagram of Tween series surfactants [27].

Figure 4 shows that the interparticle cohesive force in the presence of Tween 65, Tween 85, Tween 60, and Tween 20 surfactants with HLB values of 10.5, 11.0, 14.9, and 16.7, respectively, was higher than that of the pure cyclopentane hydrate and increased with increasing surfactant concentration. The rate of increase ranged from 11% to 207%. Higher HLB values of the surfactant resulted in a greater interparticle cohesion.

To sum up, for the Span series of surfactants with HLB values lower than 10 (i.e., hydrophobic), the cohesive force decreased with decreasing HLB and increasing surfactant concentration, but the corresponding changes were relatively small. For the hydrophilic Tween surfactants with HLB > 10, the cohesive force increased with increasing HLB and surfactant concentration. In the case of Tween 65 and Tween 85 with HLB values of 10.5 and 11.0, respectively, the cohesive force between hydrate particles increased slightly with increasing surfactant concentration. On the other hand, for the Tween 60 and Tween 20 surfactants with HLB values of 14.9 and 16.7, respectively, the interparticle cohesive force increased significantly with increasing surfactant concentration, and the maximum increase could reach 207%. The changes in the cohesion between hydrate particles with the HLB value indicate that surfactants with different HLB values have a different adsorption behavior due to their different hydrophilic/hydrophobic characteristics, and the surface properties of the hydrate particles are different.

3.1.2. Analysis of Cohesive Force between Hydrate Particles

Gas hydrate particles can aggregate via collision, and their aggregation characteristics can be explored by examining the parameters describing the cohesion between particles [28–30]. Based on previous reports, the liquid bridge force is the main component of the cohesive force between hydrate particles [31–33], and the latter can be analyzed by using the capillary liquid bridge model, as shown in Figure 5. In this study, the size of the two colliding hydrate particles is the same, which enables the accurate analysis of the mechanism by which surfactant adsorption influences the cohesion between hydrate particles.

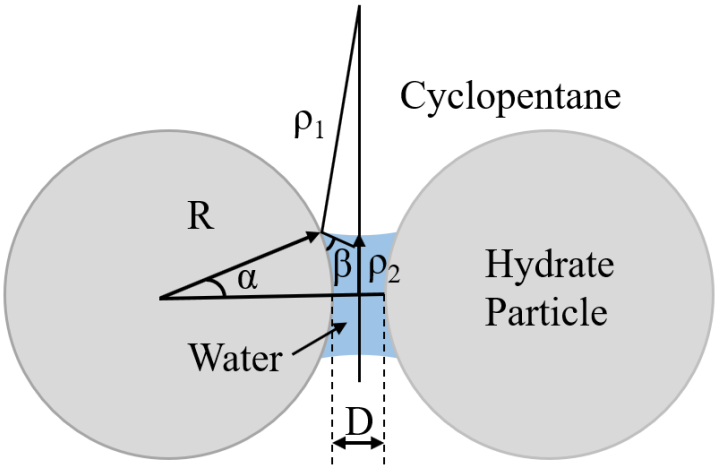

Figure 5. Schematic diagram of liquid bridge between hydrate particles. R^* is the radius of the hydrate particle (m); μ is the viscosity of the liquid inside the liquid bridge (P·s); D is the interparticle distance (m); α and β are the half-filling and contact angles (degree); ρ_1 is the radius of curvature of the outer contour of the liquid bridge (m); ρ_2 is the neck radius of the liquid bridge (m).

The liquid bridge between particles is a meniscus-shaped ring, which will produce an interface with a non-constant mean curvature. The Gorge method can be used to calculate the force of the liquid bridge; the error of this calculation is within 10%. The corresponding equation is as follows:

$$F_{Gorge} = 2\pi\rho_2\mu + \pi{\rho_2}^2\Delta P = \pi\mu\rho_2\left[1 + \frac{\rho_2}{\rho_1}\right] \quad (3)$$

where F_{Gorge} is the calculated value of liquid bridge force, (mN/m); ΔP is the pressure difference on both sides of the curved liquid surface, (Pa); μ is the viscosity of the liquid inside the liquid bridge, (P·s); and ρ_1 and ρ_2 are the radius of curvature of the outer contour of the liquid bridge (m) and the neck radius of the liquid bridge (m), and can be calculated by the following formulas.

$$\rho_1 = \frac{\frac{D}{2} + R^*(1 - cos\alpha)}{cos(\alpha + \beta)} \quad (4)$$

$$\rho_2 = R^* sin\alpha - [1 - sin(\alpha + \beta)]\rho_1 \quad (5)$$

where R^* is the radius of the hydrate particle (m); D is the interparticle distance (m); and α and β are the half-filling and contact angles (degree).

Because the hydrate particle size and spacing were different in each experiment, each group of data was calculated separately from the current experimental data. In the cyclopentane–water system, the liquid–liquid interfacial tension was 0.03 N/m, the liquid bridge fluid was water, and the viscosity was 1.8×10^{-3} Pa·s at 0 °C.

As shown in Figure 6, the cohesive force between hydrate particles increases with the increase of the HLB value. When the HLB value is 4. 3, the cohesive force is 2.32 mN/m, and when the HLB value is 16.7, the cohesive force is 5.42 mN/m. In addition, the measured value of the cohesive force between the cyclopentane hydrate particles was consistent with that calculated with the liquid bridge force model, and the error ranged between 2.67% and 12.15%, with an average of 8.17%.

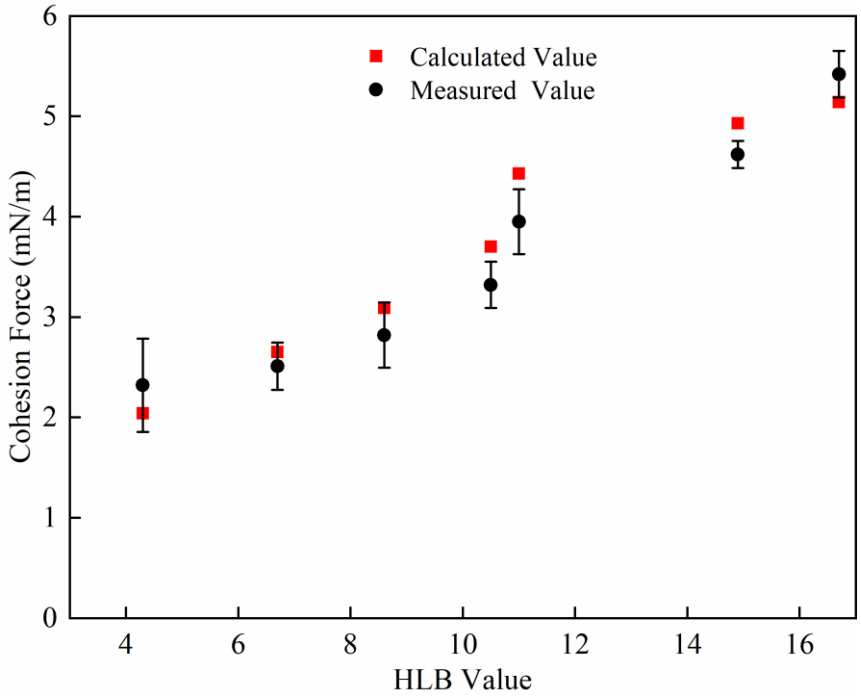

Figure 6. Variations of cohesive force between cyclopentane hydrates as a function of HLB value.

3.2. Influence Mechanism of Surfactants with Different HLB Values on Cohesive Force between Hydrate Particles

3.2.1. Change of Particle Surface Morphology

Figure 7 shows the morphology of cyclopentane hydrate particles in the presence of different surfactants, as observed with a microscope. The figure shows that the particle surface was smooth under the action of high-HLB surfactants (Figure 7e–h, corresponding to surfactants with HLB values of 10.5, 11.0, 14.9, and 16.7, respectively), while low-HLB surfactants (Figure 7b–d) resulted in a rougher particle surface. Surfactants with HLB values of 4.3, 6.7, and 8.6 caused an increased surface roughness, which affected the cohesion between particles.

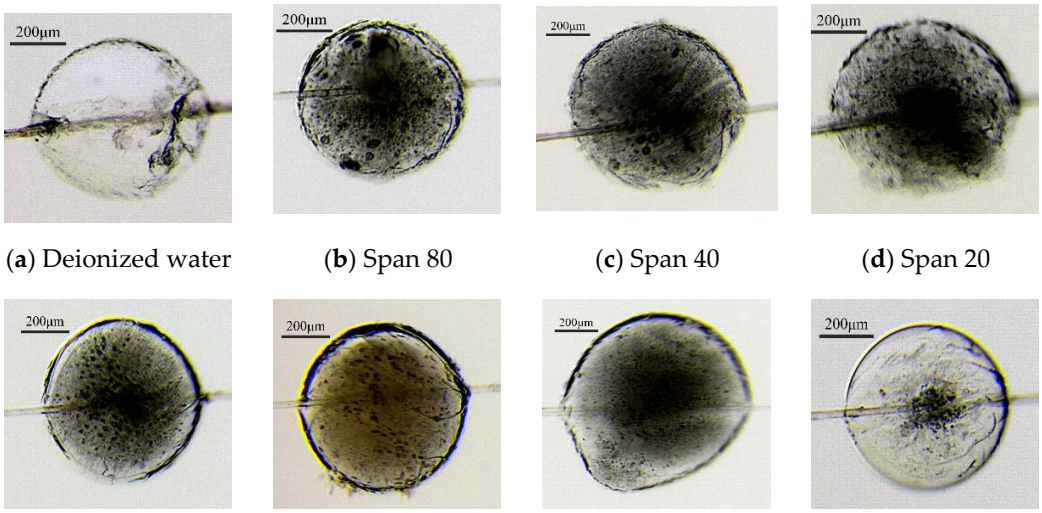

(**a**) Deionized water (**b**) Span 80 (**c**) Span 40 (**d**) Span 20

(**e**) Tween 65 (**f**) Tween 85 (**g**) Tween 60 (**h**) Tween 20

Figure 7. Morphology of cyclopentane hydrate particles in contact with different surfactants (0.1 wt.%).

The formation of hydrate particles in a surfactant-containing wellbore fluid is influenced by the solubility of the surfactant in water. The higher the HLB value of the surfactant, the stronger its hydrophilicity and the more the surfactant will dissolve in the interior of the droplet; the surfactant molecules can thus be uniformly distributed in the interior and surface regions of the droplet, which can then grow into more uniform and smooth hydrate particles in cyclopentane. Surfactants with low HLB values are strongly hydrophobic, and their solubility in water is low; this leads to their uneven dispersion in the droplet, with higher aggregation in the surface region, which affects the formation process of cyclopentane hydrate particles and leads to particles with a rough surface.

3.2.2. Changes in Particle Surface Wettability

Figure 8a shows that the cyclopentane hydrate particles possessed a strongly hydrophilic surface; on the one hand, this facilitates contact with water droplets to induce the formation of hydrate particles and increase the particle size of hydrate aggregates; on the other hand, the surface also favors the liquid bridge formation, which significantly increases the cohesion between particles and increases the risk of wellbore plugging. As shown in Figure 8b–e, the hydrate particle surface exhibited hydrophilic characteristics in the presence of the Tween series surfactants, and the wetting angle decreased with increasing HLB value of the surfactant. In particular, smaller wetting angles resulted in a larger neck radius of the liquid bridge between particles and in a stronger cohesion between them.

As shown in Figure 8f–h, the surface wettability of hydrate particles changed from hydrophilic to hydrophobic under the action of Span surfactants. The surface of hydrate particles was still hydrophilic in the presence of Span 20; however, upon contact with Span 40 and Span 80, the surfaces of the hydrate particles showed a strong hydrophobicity, and their roughness increased significantly, which indicated that a large number of Span 40 and Span 80 molecules accumulated on the surface of the droplet, affecting the formation of hydrate particles, which in turn altered their surface morphology.

Hydrate particles are formed by the transformation of liquid droplets containing surfactants, and the different hydrophilicities/hydrophobicities of surfactants with different HLB values lead to different distribution states in the droplets. Surfactants with high HLB values are uniformly distributed in the interior and surface of the droplet, while low-HLB surfactants mainly accumulate on the surface of the droplet, that is, at the air–water or oil–water interface.

Dieker and Aspenes [34] found that the risk of hydrate aggregation can be reduced by changing the surface wettability of hydrate particles from hydrophilic to hydrophobic. In the present study, when a droplet transforms into cyclopentane hydrate particles after freezing, the surfactant molecules will maintain their position in the droplet. Cyclopentane was chosen as the medium in the experiments. When the solidified particles were placed in cyclopentane within the reactor, the hydrophobic groups of the surfactant extended into the cyclopentane phase, thus forming a hydrophobic region on the particle surface. In deepwater oil/gas and hydrate drilling/production as well as in oil/gas gathering pipelines, the dispersion medium is natural gas or oil; when the pipeline is injected with an anti-agglomerant solution, the surfactant participating in the formation of hydrate particles will also tend to extend its hydrophobic groups to the oil phase or alkane gas, thus forming hydrate particles with hydrophobic surfaces. Surfactants with low HLB values have strong hydrophobicity, and the surface of hydrate particles formed under the action of the surfactant is hydrophobic. Therefore, cyclopentane hydrate particles formed in the presence of Span 80, Span 40, and Span 20 exhibit lower interparticle forces, mainly because of the formation of hydrate particles with hydrophobic surfaces.

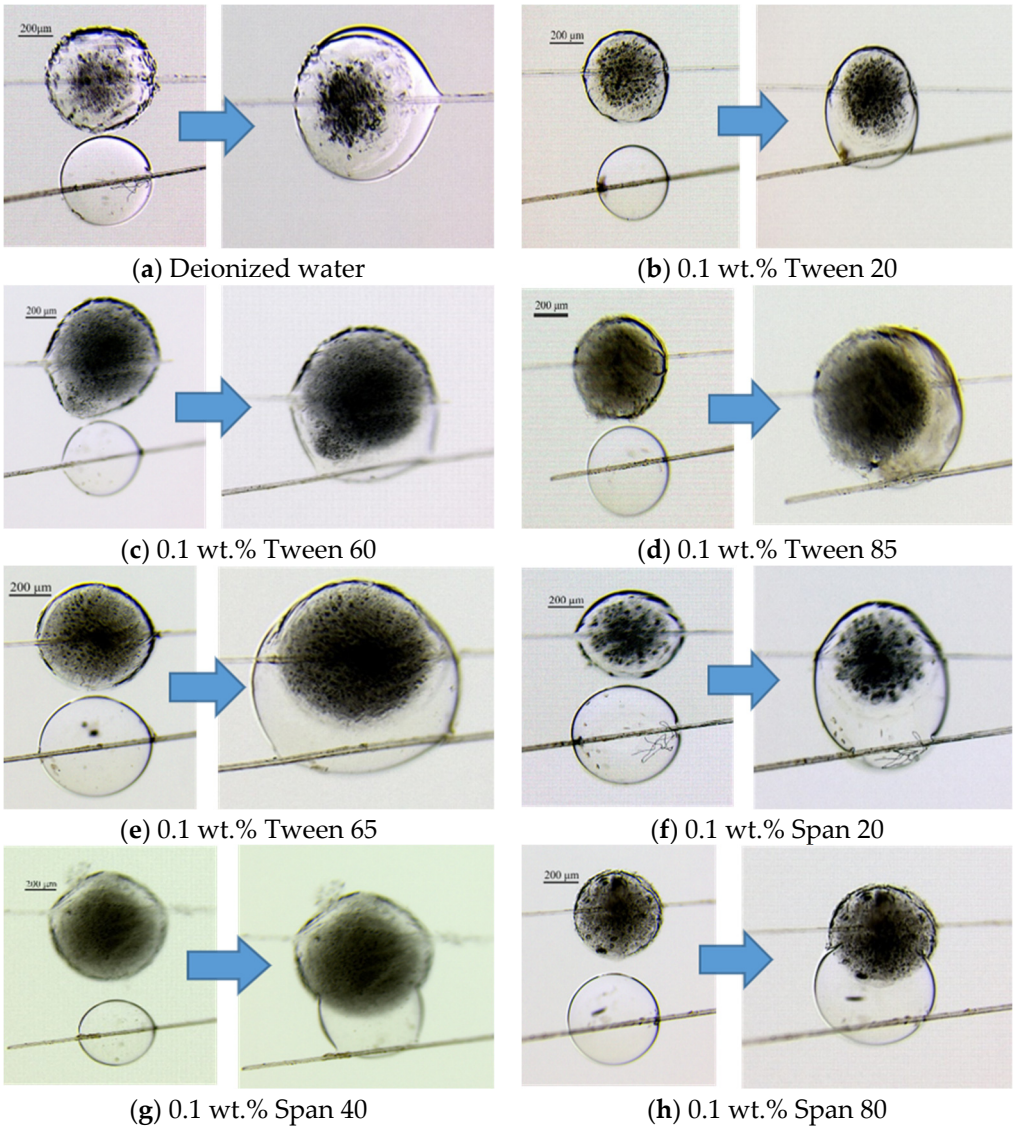

(**a**) Deionized water (**b**) 0.1 wt.% Tween 20

(**c**) 0.1 wt.% Tween 60 (**d**) 0.1 wt.% Tween 85

(**e**) 0.1 wt.% Tween 65 (**f**) 0.1 wt.% Span 20

(**g**) 0.1 wt.% Span 40 (**h**) 0.1 wt.% Span 80

Figure 8. Wettability tests in the presence of surfactants with different HLB values.

Surfactants with high HLB values have strong hydrophilicity and disperse more uniformly in the water phase, while low-HLB surfactants have strong hydrophobicity and preferentially accumulate on the surface of droplets. Therefore, at a constant surfactant concentration, lower HLB values correspond to a higher hydrophobicity of the surfactant, resulting in more hydrophobic hydrate particles; as a result, the interparticle force decreases with decreasing HLB. In the case of a constant HLB value, the hydrophilicity/hydrophobicity of the hydrate particles increases with increasing surfactant concentration. As the concentration of surfactant with high HLB increases, the number of hydrophilic surfactant molecules adsorbed and aggregated on the surface of hydrate particles increases, thus increasing the surface hydrophilicity and cohesion. On the other hand, increasing the concentration of low-HLB surfactants results in a higher number of hydrophobic surfactant molecules adsorbed and aggregated on the surface; thus, the surface hydrophobicity of the hydrate particles increases and the cohesion decreases.

3.3. Analysis of Microscopic Mechanism of Inhibition of Hydrate Particle Aggregation

The above results on the relationship between hydrate particle morphology, wettability, and interparticle force under the action of Span surfactants show that the use of low-HLB surfactants can endow the surface of hydrate particles with hydrophobic characteristics, which are expected to prevent hydrate particles from aggregating and causing blockages in wellbores. The surface of hydrate particles formed in the presence of Span 40 and Span 80 is hydrophobic, and the cohesion between particles is low, which can prevent their aggregation. The preliminary analysis of the underlying mechanism is shown in Figure 9.

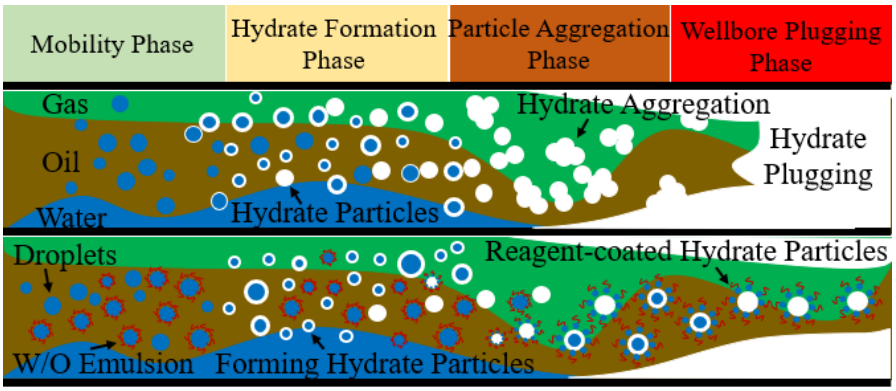

Figure 9. Schematic diagram of inhibition of hydrate particle aggregation by Span series surfactants (without and with Span surfactants, respectively).

In systems containing oil, Span surfactants can emulsify water droplets to form water-in-oil (W/O) emulsions and prevent their contact with hydrate particles. On the other hand, the incorporation of five-membered rings in the hydrophilic head of the surfactant can affect the formation of hydrate particles and enable surfactant adsorption on their surface; at the same time, the hydrophobic tail group extends from the hydrate surface to the liquid phase, which alters the wettability of the particle surface, reducing the adhesive force between particles; this results in the particles producing steric hindrance and disperse in the gas–water system of the wellbore, thereby achieving the purpose of preventing hydrate aggregation and further avoiding blockage.

The addition of Tween series surfactants enhances the wettability of hydrate particles, and the wetting angle between water droplets and hydrate particles decreases with increasing surfactant HLB. The degree of wettability cannot be used to directly characterize the extent of cohesion between particles but can affect the volume of the liquid bridge between hydrate particles, which is positively correlated with the liquid bridge force between the particles. According to the calculations based on the liquid bridge model between hydrate particles (Equation (3)), as the wetting angle decreases, the neck radius of the liquid bridge increases; in other words, the volume of the liquid bridge increases, resulting in a higher

cohesion between hydrate particles. Therefore, in the presence of Tween series surfactants, as the HLB value increases, the neck radius and volume of the liquid bridge between particles increase, resulting in a stronger cohesion between particles. As shown in Figure 10, a higher surfactant concentration results in a larger volume and thus a stronger cohesion.

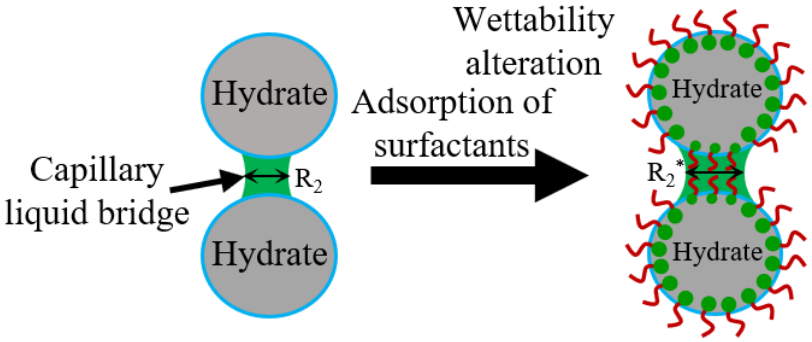

Figure 10. Mechanism of increase in interparticle cohesion by Tween series surfactants.

4. Conclusions

Measurements of the cohesive force between cyclopentane hydrate particles show that in the presence of four hydrophilic Tween surfactants with HLB values higher than 10 (HLB = 10.5, 11.0, 14.9, and 16.7) and three hydrophobic Span surfactants with HLB values lower than 10 (HLB = 4.3, 6.7, and 8.6), the cohesive force decreased with decreasing HLB; the experimental results were in good agreement with the results of calculations based on the liquid bridge force model. Using hydrophilic Tween surfactants, the cohesive force between cyclopentane hydrate particles increased with increasing surfactant concentration. In the case of hydrophobic Span surfactants, the cohesive force decreased with increasing concentration. During the formation of cyclopentane hydrate particles, the aggregation of surfactant molecules with low HLB value at the oil–water or gas–water interface altered the surface roughness and wettability of hydrate particles. Because the interaction between hydrate particles mainly originates from liquid bridge forces, the surface changed from hydrophilic to hydrophobic, which inhibited the formation of the liquid bridge, and then reduced the cohesive force between cyclopentane hydrate particles, thus reducing hydrate aggregation and blockage risks. Therefore, the design and selection of surfactants with low HLB values as anti-agglomerants may be an effective way to prevent hydrate particles from aggregating.

Author Contributions: Conceptualization, X.Z. and Z.W.; methodology, X.Z. and Q.F.; formal analysis, X.Z. and Q.F.; investigation, Q.F., S.L. and Q.G.; resources, Z.Q. and Z.W.; data curation, Q.F. and S.L.; writing—original draft preparation, Q.F.; writing—review and editing, X.Z.; supervision, Z.Q., Z.W. and X.Z.; funding acquisition, Z.Q. and Z.W. All authors have read and agreed to the published version of the manuscript.

Funding: This work was supported by the National Natural Science Foundation of China (51991363; 51804331), the CNPC's Major Science and Technology Projects (ZD2019-184-003).

Institutional Review Board Statement: Not applicable.

Informed Consent Statement: Not applicable.

Data Availability Statement: Not applicable.

Conflicts of Interest: The authors declare no conflict of interest.

References

1. Makogon, Y.F. Natural gas hydrates-A promising source of energy. *J. Nat. Gas Sci. Eng.* **2010**, *2*, 49–59. [CrossRef]
2. Ghavipour, M.; Ghavipour, M.; Chitsazan, M.; Najibi, S.H.; Ghidary, S.S. Experimental study of natural gas hydrates and a novel use of neural network to predict hydrate formation conditions. *Chem. Eng. Res. Des.* **2013**, *91*, 264–273. [CrossRef]

3. Musakaev, N.G.; Khasanov, M.K.; Borodin, S.L. The mathematical model of the gas hydrate deposit development in permafrost. *Int. J. Heat Mass Transf.* **2018**, *118*, 455–461. [CrossRef]
4. Jassim, E.; Abdi, M.A.; Muzychka, Y. A new approach to investigate hydrate deposition in gas-dominated flowlines. *J. Nat. Gas Sci. Eng.* **2010**, *2*, 163–177. [CrossRef]
5. Farhadian, A.; Varfolomeev, M.A.; Rezaeisadat, M.; Semenov, A.P.; Stoporev, A.S. Toward a bio-based hybrid inhibition of gas hydrate and corrosion for flow assurance. *Energy* **2020**, *210*, 118549. [CrossRef]
6. Yang, M.; Zhao, J.; Zheng, J.N.; Song, Y.C. Hydrate reformation characteristics in natural gas hydrate dissociation process: A review. *Appl. Energy* **2019**, *256*, 113878. [CrossRef]
7. Long, Z.; Zhou, X.B.; He, Y.; Li, D.L.; Liang, D.Q. Performance of mixture of ethylene glycol and glycine in inhibiting methane hydrate formation. *J. Nat. Gas Sci. Eng.* **2018**, *56*, 134–140. [CrossRef]
8. Taylor, C.J.; Dieker, L.E.; Miller, K.T.; Koh, C.A.; Sloan, E.D. Micromechanical cohesion force measurements between tetrahydrofuran hydrate particles. *J. Colloid Interface Sci.* **2007**, *306*, 255–261. [CrossRef]
9. Sloan, E.D. *Natural Gas Hydrates in Flow Assurance*; Gulf Professional Publishing: Amsterdam, The Netherlands, 2010.
10. Shi, B.; Song, S.; Chen, Y.; Duan, X.; Liao, Q.Y.; Fu, S.K.; Liu, L.H.; Sui, J.H.; Jia, J.P.; Liu, H.T.; et al. Status of Natural Gas Hydrate Flow Assurance Research in China: A Review. *Energy Fuels* **2021**, *35*, 3611–3658. [CrossRef]
11. Lei, S.F.; Sun, J.S.; Lv, K.H.; Zhang, Q.T.; Yang, J.B. Types and Performances of Polymer Gels for Oil-Gas Drilling and Production: A Review. *Gels* **2022**, *8*, 386. [CrossRef]
12. Kelland, M.A. History of the development of low dosage hydrate inhibitors. *Energy Fuels* **2006**, *20*, 825–847. [CrossRef]
13. Klomp, U.C.; Reijmhart, R. Method for Inhibiting the Plugging of Conduits by Gas Hydrates. WO Patent Application 95/17579, 1995.
14. Sun, M.W.; Firoozabadi, A. New surfactant for hydrate anti-agglomeration in hydrocarbon flowlines and seabed oil capture. *J. Colloid Interface Sci.* **2013**, *402*, 312–319. [CrossRef] [PubMed]
15. Saikia, T.; Mahto, V. Evaluation of Soy Lecithin as Eco-Friendly Biosurfactant Clathrate Hydrate Anti-agglomerant Additive. *J. Surfactants Deterg.* **2018**, *21*, 101–111. [CrossRef]
16. Zhao, X.; Fang, Q.C.; Qiu, Z.S.; Mi, S.Y.; Wang, Z.Y.; Geng, Q.; Zhang, Y.B. Experimental investigation on hydrate anti-agglomerant for oil-free systems in the production pipe of marine natural gas hydrates. *Energy* **2022**, *242*, 122973. [CrossRef]
17. Kelland, M.A.; Svartaas, T.M.; Dybvik, L. Studies on New Gas Hydrate Inhibitors. In Proceedings of the SPE Offshore Europe, Aberdeen, UK, 5 September 1995.
18. Kelland, M.A.; Svartaas, T.M.; Dybvik, L. A New Generation of Gas Hydrate Inhibitors. In Proceedings of the SPE Annual Technical Conference and Exhibition, Dallas, TX, USA, 22 October 1995.
19. Huo, Z.; Freer, E.; Lamar, M.; Sannigrahi, B.; Knauss, D.M.; Sloan, E.D. Hydrate plug prevention by anti-agglomeration. *Chem. Eng. Sci.* **2001**, *56*, 4979–4991. [CrossRef]
20. Koh, C.A.; Westacott, R.E.; Zhang, W.; Hirachand, K.; Creek, J.L.; Soper, A.K. Mechanisms of gas hydrate formation and inhibition. *Fluid Phase Equilibria* **2002**, *194–197*, 143–151. [CrossRef]
21. Fan, X.; Ten, P.; Clarke, C.; Bramley, A.; Zhang, Z. Direct measurement of the adhesive force between ice particles by micromanipulation. *Powder Technol.* **2003**, *131*, 105–110. [CrossRef]
22. Yang, S.O.; Kleehammer, D.M.; Huo, Z.X.; Sloan, E.D.; Miller, K.T. Temperature dependence of particle–particle adherence forces in ice and clathrate hydrates. *J. Colloid Interface Sci.* **2004**, *277*, 335–341. [CrossRef]
23. Hu, S.J.; Vo, L.; Monteiro, D.; Bodnar, S.; Prince, P.; Koh, C.A. Structural Effects of Gas Hydrate Antiagglomerant Molecules on Interfacial Interparticle Force Interactions. *Langmuir* **2021**, *37*, 1651–1661. [CrossRef]
24. Wang, S.L.; Fan, S.S.; Lang, X.M.; Wang, Y.H.; Wang, P.F. Particle size dependence of clathrate hydrate particle cohesion in liquid/gaseous hydrocarbons. *Fuel* **2020**, *259*, 116201. [CrossRef]
25. Chen, Z.H.; Liu, B.; Manica, R.; Liu, Q.X.; Xu, Z.H. Interaction Between the Cyclopentane Hydrate Particle and WaterDroplet in Hydrocarbon Oil. *Langmuir* **2020**, *36*, 2063–2070. [CrossRef] [PubMed]
26. Aman, Z.M.; Joshi, S.E.; Sloan, E.D.; Sum, A.K.; Koh, C.A. Micromechanical cohesion force measurements to determine cyclopentane hydrate interfacial properties. *J. Colloid Interface Sci.* **2012**, *376*, 283–288. [CrossRef] [PubMed]
27. Feltes, M.M.C.; Villeneuve, P.; Barea, B.; Oliveira, D.D.; Ninow, J.L. Evaluation of the use of surfactants as additives in enzymatic glycerolysis reactions. *Eur. J. Lipid Sci. Technol.* **2012**, *114*, 1352–1357. [CrossRef]
28. Brown, E.P.; Koh, C.A. Micromechanical measurements of the effect of surfactants on cyclopentane hydrate shell properties. *Phys. Chem. Chem. Phys* **2016**, *18*, 594–600. [CrossRef] [PubMed]
29. Pitois, O.; Moucheront, P.; Chateau, X. Liquid Bridge between Two Moving Spheres: An Experimental Study of Viscosity Effects. *J. Colloid Interface Sci.* **2000**, *231*, 26–31. [CrossRef] [PubMed]
30. Dieker, L.E.; Aman, Z.M.; George, N.C.; Sum, A.K.; Sloan, E.D.; Koh, C.A. Micromechanical Adhesion Force Measurements between Hydrate Particles in Hydrocarbon Oils and Their Modifications. *Energy Fuels* **2009**, *23*, 5966–5971. [CrossRef]
31. Aspenes, G.; Høiland, S.; Barth, T.; Askvik, K.M. The influence of petroleum acids and solid surface energy on pipeline wettability in relation to hydrate deposition. *J. Colloid Interface Sci.* **2009**, *333*, 533–539. [CrossRef]
32. Aspenes, G.; Dieker, L.E.; Aman, Z.M.; Høiland, S.; Sum, A.K.; Koh, C.A.; Sloan, E.D. Adhesion force between cyclopentane hydrates and solid surface materials. *J. Colloid Interface Sci.* **2010**, *343*, 529–536. [CrossRef]

33. Al Brahim, A.; Bai, B.J.; Schuman, T. Comprehensive Review of Polymer and Polymer Gel Treatments for Natural Gas-Related Conformance Control. *Gels* **2022**, *8*, 353. [CrossRef]
34. Wang, T.F.; Wang, L.L.; Qin, H.L.; Zhao, C.; Bai, Z.X.; Meng, X.B. Identification of Gas Channeling and Construction of a Gel-Enhanced Foam Plugging System for Oxygen-Reduced Air Flooding in the Changqing Oilfield. *Gels* **2022**, *8*, 373. [CrossRef]